Ultra-Low Global Warming Potential Heat Transfer Fluids for Pumped Two-Phase Cooling in HPC Data Centers

Nitin Karwa
Honeywell International Inc.,
Honeywell India Technology Center,
Gurgaon, India, 122018
Email: Nitin.Karwa@Honeywell.com

ABSTRACT

The increasing heat dissipation from microprocessors and power density of racks in high performance computing (HPC) applications necessitates liquid cooling of the microprocessors in the servers. Currently, water and aqueous glycol are primarily used as coolants. The need to sustain ever-increasing power density, inherent risks and inefficiencies with water cooling, and the push towards lower global warming potential dielectric fluids, has motivated a search for suitable two-phase heat transfer fluids. This study presents evaluation of pumped single-phase water cooling and two-phase cooling in microchannel cold plate. The water cooling was tested at mass flow rate of up to 125 kg/h. Two-phase cooling with R134a and ultra-low Global Warming Potential (GWP) dielectric fluids R1233zd(E) and R1234ze(E) was tested at mass flow rates of up to 30 kg/h and heat fluxes up to 640 kW/m^2. Compared to water cooling, two-phase cooling achieves lower junction temperatures and more uniform cooling for the same flow rates. When compared at equal junction temperature, two-phase cooling requires an order of magnitude lower pumping power than water cooling. This study demonstrates that two-phase cooling with R1233zd(E) and R1234ze(E) can be feasible options compared to water cooling in HPC data centers.

KEY WORDS: microchannel cold plate, water, R1233zd(E), R1234ze(E), R134a, hydrofluoroolefins, thermal resistance

NOMENCLATURE

A_H	heated area, m^2
Co	confinement number, –
D_H	hydraulic diameter, m
g	acceleration due to gravity (9.81), m/s^2
G	mass flux, kg/(m^2·s)
h	specific enthalpy, J/kg
H	channel height, m
I	current, A
k	thermal conductivity, W/(m·°C)
L	channel length, m
$\dot{m}$	mass flow rate, kg/s
N	number of channels, -
$\ddot{q}$	heat flux, W/m^2
Q	heat input, W
R	thermal resistance, °C/W
t	thickness of base, m
T	temperature, ºC
V	voltage, V
W	channel width, m
W_f	fin width, m
x	vapor quality, -

Greek symbols

μ	viscosity, Pa·s
ρ	mass density, kg/m^3
σ	surface tension, N/m

Subscripts

B	base
CU	copper
IN	inlet
J	junction
L	liquid
LV	latent
OUT	outlet
SAT	saturation
V	vapor

INTRODUCTION

The increasing power levels of microprocessors and the use of racks with heat loads exceeding 30 kW in high performance computing (HPC) applications necessitates direct liquid cooling of the microprocessors in the servers. Liquid cooling not only allows effective heat removal compared to air cooling, but the coolant inlet temperatures can also be raised above the outdoor air temperature even in hot climates such that year-round free-cooling can be achieved. Liquid cooling is achieved by either submerging the electronics into a pool of heat transfer fluid, also referred as immersion cooling, or attaching a liquid-cooled cold plate to the surface of the electronics. Only dielectric fluids can be used in immersion cooling while cold plate cooling uses both non-dielectric fluids, e.g., water and aqueous glycol, and dielectric fluids, e.g., fluorinated liquids and mineral oils.

Water and aqueous glycol are only used as single-phase heat transfer fluids. There are several inherent risks and inefficiencies with pumped water cooling. Water is corrosive and prone to biological growth; therefore, the water quality management is crucial. Additives such as corrosion inhibitors and biocides are added to water, yet online monitoring and periodic testing of samples is necessary. Despite these measures, only copper and stainless steel are used due to corrosion issues. Periodic leak checks and extensive leak detection systems are necessary to avoid equipment damage in the case of a leak. HPC servers have multiple central processing units (CPU) and graphical processing units (GPU). Water is distributed to the cold plates attached to these devices in both series and parallel loops. When cold plates are connected in series, water temperature increases as it flows through a cold plate and the performance of the next inline cold plate is penalized, often called as thermal shadowing. On the other hand, when cold plates are connected in parallel in the cooling loop, the flow rate and the tube diameter increase, which

reduces the packing density of the server [1]. Additionally, the above noted issues limit the smallest microchannel size in cold plates, thereby limiting its effectiveness for future high thermal design power (TDP) devices. It is recommended to use an in-line filter with an absolute filter rating of 7 to 10 times smaller than the finest microchannel dimension in the cold plate [2].

Two-phase cooling using dielectric fluids may be able to overcome several of these challenges. For example, fluorinated hydrocarbons such as hydrofluoroolefins (HFO) are compatible with almost all metals and do not have issues such as biofouling and choking of microchannels. Leak detection of HFO is easy as the liquid quickly flashes into vapor when it leaks out of the system and even low concentration of vapor inside the server and the coolant distribution unit can be detected using sensors. Two-phase cooling with fluid having low saturation temperature drop will eliminate thermal shadowing. This paper also demonstrates that two-phase cooling requires much lower mass flow rates than single-phase water cooling to achieve same or better thermal resistance. Therefore, two-phase cooling requires narrow tubes as compared to single-phase water cooling, which makes tubing layout more manageable and frees up space on the motherboard for more devices.

Heat transfer fluids for two-phase cooling

Fluorinated fluids such as hydrofluorocarbons (HFC), hydrofluoroolefins (HFO), hydrofluoroethers (HFE) and fluoroketones (FK) have been investigated as potential heat transfer fluids for electronics cooling. Fluorinated fluids that are non-flammable, having high dielectric strength, no ozone depletion potential, low global warming potential (GWP) and toxicity, and that can provide excellent heat transfer properties would be most suitable for the application. Pumped two-phase cooling with R134a is already used for industrials electronics. Ultra-low GWP refrigerants R1234ze(E) and R1234yf, are replacement refrigerants for R134a, primarily developed for chiller applications and mobile air conditioning, respectively. Generally, the maximum working pressure of pumped water systems is limited to about 100 psi. R1233zd(E), with system pressure of 45 psi at 50 °C, may be a replacement fluid for water. The basic properties of the above heat transfer fluids are listed in Table 1. High liquid density and latent heat reduce the volume flow rate required to remove a given heat load. High latent heat of vaporization and vapor to liquid density ratio increases the critical heat flux. Low viscosity and high vapor density reduce the pressure drop, while high thermal conductivity of liquid improves the heat transfer coefficient.

Two-phase cooling in microchannels

According to Ong and Thome [4], macro-to-microscale transition criterion for two-phase flow in channels can be defined based on the confinement number Co. Confinement number is defined as

$$Co = \frac{1}{D_H}\sqrt{\frac{\sigma}{g(\rho_L - \rho_V)}} \quad (1)$$

where hydraulic diameter, D_H, of the microchannel defined as

$$D_H = \frac{2WH}{W+H} \quad (2)$$

They defined the lower boundary of macroscale flow as $Co < 0.3 - 0.4$ and the upper boundary of symmetric microscale flow as $Co > 1$. Asymmetric microscale flow regime is between $0.3 - 0.4 \leq Co \leq 1$.

Table 1. Fluid and environmental properties of heat transfer fluids evaluated for two-phase cooling at a saturation temperature of 52°C unless otherwise specified. The fluid properties and vapor pressure were obtained using NIST property database REFPROP 9.1 [3].

Property	R134a	R1234ze(E)	R1233zd(E)
Molecular formula	CF3-CH2F	(E)CF3-CH=CHF	(E)CF3-CH=CCIH
GWP[a]	1300	<1	1
OELs, ppm	1000	1000	800
Flammability[b]	Nonflammable	Nonflammable	Nonflammable
Boiling point at 1 atm., ºC	-26.07	-18.97	18.26
ASHRAE Std. 34 safety classification[c]	A1	A2L	A1
Pressure, kPa	1385	1049	311.2
ρ_L, kg/m^3	1093	1065	1194.4
ρ_V, kg/m^3	70	56.5	16.6
h_{LV}, kJ/kg	149.4	143.7	176.1
k_L, W/m·°C	0.069	0.065	0.068
k_V, W/m·°C	0.017	0.016	0.012
μ_L, μPa·s	138	144.43	335
μ_V, μPa·s	13	13.57	12.06
σ, mN/m	4.67	5.5	11.1

[a] IPCC fifth assessment report (GWP CO_2 = 1)
[b] Flammability test according to ASTM E681-04 at 21 ºC
[c] Flammability test according to ASTM E681-2009 at 60 ºC

Revellin and Thome [5] have observed three flow regimes for R134a and R245fa flow in microchannels, namely, isolated bubble, coalescing bubble and smooth-annular flow. They found that along the length of the channel, the flow first transitions from intermittent to coalescing bubble flow regime and then to annular flow regime. As channel confinement increases, these transitions occur at lower vapor qualities [4]. Costa-Patry et al. [6] experimentally determined the two-phase heat transfer coefficient distribution for R134a, R1234ze(E) and R245fa along the channels of a microchannel cold plate with the exit vapor quality up to 0.6. They observed that the heat transfer coefficient first decreases along the channel, reaches a minimum value and then starts to again increase. They found that the vapor quality at the minimum heat transfer coefficient nearly coincides with the coalescing bubble flow regime to annular flow regime transition. The vapor quality at minimum heat transfer coefficient increases with heat flux and decreases with mass flux. They developed a flow pattern-based model that was able to capture the trends of the local heat transfer distribution, but the mean absolute error was higher

than 20%. On the other hand, flow boiling correlations that are based on a weighted combination of nucleate boiling and convective heat transfer, such as that of Bertsch et al. [7], predict a nearly flat or decreasing trend of heat transfer coefficient along the channel with higher error in predicting average heat transfer coefficient. They reported that R1234ze(E) and R134a have comparable pressure drops, while the pressure drops for R245fa are up to four times that of R134a due to its lower vapor to liquid density ratio. Comparison of heat transfer coefficient for R1234ze(E) and R134a is reported only at one operating condition. It was reported that R1234ze(E) offers higher heat transfer coefficient than R134a, and R245fa has the lowest heat transfer coefficient.

Huang et al. [8] reported the thermohydraulic behavior of R1233zd(E) in a microchannel cold plate. Their study focused on evaluating the pressure drop and local heat transfer coefficient distribution in high mass flux regime where transition to annular flow happens close to the inlet of the channel at local vapor quality of ~0.05. They observed that the channel pressure drop increased with the mass flux and vapor quality. They confirmed that flow pattern-based model captures the trends of the local heat transfer distribution.

Fayyadh et al. [9] and Madhour et al. [10] reported that average heat transfer coefficient for R134a in a parallel microchannel cold plate increases with heat flux but shows a weak dependence on mass flux. Olivier and Thome [11] simulated both two-phase refrigerant and single-phase water cooling in a microchannel cold plate. They showed that R1234ze(E) performance to be a close match with R134a. The junction temperatures and base temperature uniformity for single-phase water cooling were only comparable to two-phase R134a cooling when their mass flow rates are almost an order of magnitude higher. The resulting pumping power with water cooling was up to 40 times higher than R134a.

Although two-phase passive cooling has been investigated by several researchers, no experimental study has been done to compare its performance with single-phase water cooling in the same cold plate. The objective of this paper is to present new thermal resistance and temperature non-uniformity data in multi-microchannel copper cold plate with R1233zd(E), R1234ze(E), R134a and water for thermal boundary conditions comparable to that of CPU used in HPC applications.

EXPERIMENTAL TEST SETUP AND PROCEDURE

A schematic of the pumped two-phase loop is shown in Fig. 1. The loop pressure was maintained by setting the fluid temperature within the reservoir. An oil-free variable speed external gear pump from Micropump Inc. circulated the heat transfer fluid in the loop. The mass flow rate was measured using a Coriolis mass flow meter with an accuracy of ±0.1% of the reading. Subcooled liquid was preheated in a brazed plate heat exchanger before it entered the cold plate. The heat transfer fluid gained heat as it flowed through the cold plate. The vapor rejected its heat in a brazed plate condenser, and liquid with around 5 ºC subcooling was supplied at the pump inlet. Fluid temperatures were measured using T-type thermocouples, calibrated within ±0.1 ºC. Inlet and receiver pressures were measured using two 300 psi absolute pressure transducers having an accuracy of ±0.10% of full scale (i.e., ±0.3 psi), while a ±15 psi differential pressure transducer with an accuracy of 0.1% of full scale (i.e., ±0.015 psi) was used to measure the pressure drop across the cold plate.

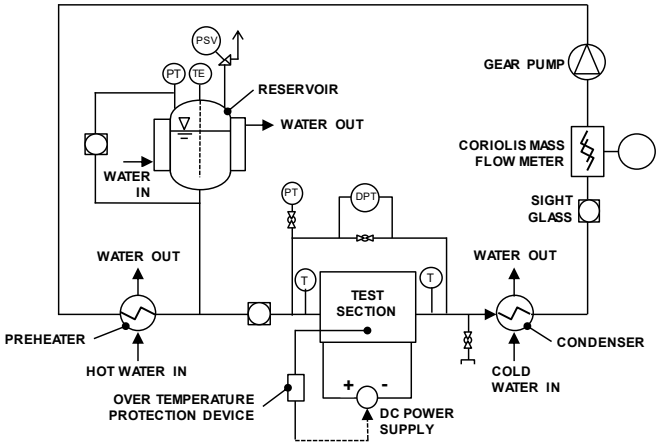

Fig. 1 Schematic of pumped two-phase cooling loop

The test section is composed of a copper block with embedded cartridge heaters, a layer of thermal interface material (TIM), and a cold plate (Fig. 2). The cold plate is mounted on the copper block using the thermal interface material having a thermal conductivity of 8.5 W/(m·°C). The cold plate is an assembly of a copper base plate, a stainless steel cover plate and a flat gasket. The copper base plate has integral high aspect ratio fins manufactured by micro deformation technology, thereby providing a smooth surface finish to the fins. When the cover plate and the base plate are assembled, parallel rectangular microchannels are formed. Dimension of the formed microchannels are given in Table 2. The microchannel surface area is calculated by considering the face formed by the cover plate to be thermally insulated. The finned area of the base plate and the face area of the copper block attached to the cold plate, A_H, is 25 × 25 sq. mm. 4 mm wide rectangular headers that span across all the microchannels are formed at either ends of the microchannels for fluid distribution. The cover plate includes manifolds for the supply and discharge of coolant to and from the headers, respectively. through ports that are parallel to the base plate. The inlet port is an orifice at one end of the inlet header and the coolant impinges normally on the base plate like a confined jet after it leaves the inlet port. This restriction formed by means of the inlet slit and the confined jet flow imposes pressure drop which reduces back flow in the cold plate. Sharma et al. [12] have observed that impinging jets in the inlet manifold are effective in delaying the formation of big vapor bubble in the inlet header. The outlet port is a rectangular slit that spans across all the microchannels and is 4 mm wide to minimize pressure loss. The inlet and outlet tubes have ¼ inch outer diameter and are 25 mm long. Pressure taps were located on the inlet and outlet tubes, while thermocouples were affixed on the outer surface of the inlet and outlet tubes and insulated with closed cell nitrile foam insulation. Shielded T-type 500 μm diameter thermocouples were embedded 1.5 mm below the bottom surface of the microchannels and the manifolds. Tip of these thermocouples were located under the geometric center of the header and finned areas (see Fig. 3).

Three cartridge heaters were embedded in the copper block and all the heaters generated the same amount of heat, which provided uniform heat generation at the base of the copper block. The sides of the copper block and the top of the cold plate were insulated with mineral wool and then enclosed with nitrile insulation. The heat transfer in the copper block is expected to be one-dimensional. The cartridge heaters were powered using a variable DC power supply. The voltage was recorded using a data acquisition unit while the current was measured and displayed directly on the power supply.

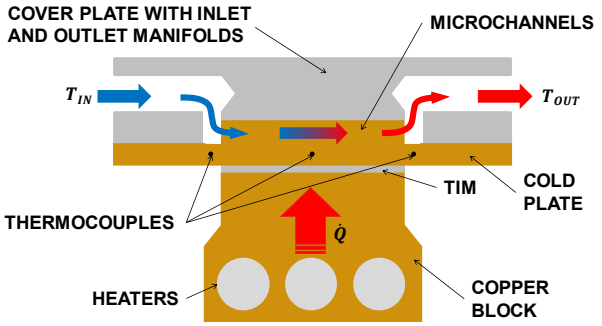

Fig. 2 Schematic of the test section showing the assembly of the cold plate with the heater block

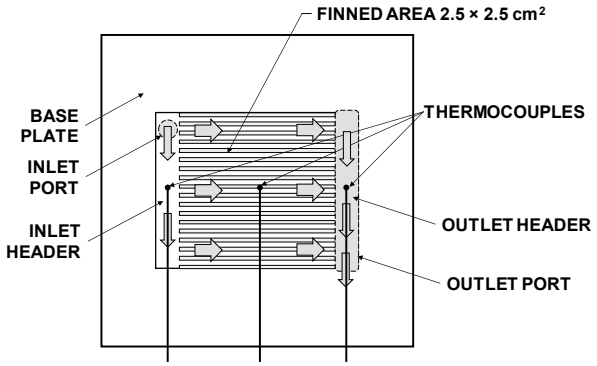

Fig. 3 Schematic of the microchannel cold plate

Table 2. Dimensions of the microchannels

Parameter	Value
Base plate thickness, t_B, mm	3
Finned area, A_H, sq. mm	25 x 25
Microchannel length, L, mm	25
Microchannel height, H, mm	2
Channel width, W, mm	0.64
Hydraulic diameter, D_H, mm	0.97
Fin width, W_f, mm	0.64
Microchannel surface area, sq. m	0.0022
Number of microchannels, N. -	19

The temperature, pressure, mass flow rate and voltage readings were acquired using a Keysight 64287 data acquisition unit at a rate of 6 samples per minute per channel. All readings were recorded under steady state condition, which was assumed to be obtained when various temperatures did not deviate by more than ±0.1 ºC of the mean value over a period of 15 minutes. The data was recorded for 10 minutes after steady state was achieved and averaged data was used in the data reduction process.

For the two-phase flow experiments, the system was purged with dry nitrogen and then evacuated until a pressure of 40 Pa was achieved before the heat transfer fluid was charged into the system as liquid. In the case of R1233zd(E), any non-condensable gases introduced into the system during charging were purged out of the system from a port at the top of the reservoir by raising the reservoir temperature 50 ºC until the reservoir pressure matched the saturation pressure at the fluid temperature. However, the experiments with water were performed in an open loop.

In each experiment, the receiver pressure was first set to the desired value and then the flow rate and temperature at the inlet of the cold plate were stabilized. The heater power supply was switched on and set to the desired value. The flow rate was gradually increased to perform all the tests at the set heat input. The heat input was then increased for the next set of tests and the procedure repeated. Except in the tests at the lowest mass flux and the highest power input, loss of cooling did not occur in the tests.

OPERATING CONDITIONS

Single-phase cooling tests with water were performed at an inlet temperature of 50 ºC, which is typical of systems designed for ASHRAE W4 class of facility inlet water-supply temperature [13]. The water flow rate ranged from 25 to 125 kg/h (mass flux ranged from 290 to 1450 kg/m^2·s and Reynolds number based on the channel hydraulic diameter ranged from 520 to 2600).

Two-phase cooling tests were performed with R1233zd(E), R1234ze(E) and R134a at inlet saturation temperature, $T_{SAT,IN}$, of 52 ± 1 °C and the inlet temperature, T_{IN}, of 50 ºC. The resulting inlet subcooling was 2 ± 1 °C. The fluid properties and vapor pressure were obtained using NIST property database REFPROP 9.1 [3]. Reservoir pressure was in close agreement with the calculated saturation pressure at the measured reservoir fluid. At the inlet saturation condition, asymmetric microscale flow occurs as the confinement number for R1233zd(E), R1234ze(E) and R134a is 1, 0.76 and 0.7, respectively. Based on the confinement number criterion proposed by Ong and Thome [4], asymmetric microscale two-phase flow can be ensured for the three tested fluids. The flow rate ranged from 6 to 30 kg/h (mass flux ranged from 70 to 350 kg/m^2·s). The vapor quality at the exit of the cold plate is calculated by applying energy balance on the cold plate. The heat input ranged from 25 and 400 W (heat flux ranged from 40 to 640 kW/m^2), which covers the full range of heat dissipated by current and future CPU in HPC applications.

DATA REDUCTION AND UNCERTAINTY ANALYSIS

The mass flux, G, is calculated as

$$G = \frac{\dot{m}}{NWH} \tag{1}$$

The heat generated in the cartridge heaters is calculated as

$$Q = VI \tag{2}$$

Heat loss from the test section was estimated in single-phase heat transfer experiments to be less than 5 W and was ignored in the subsequent analysis. Though some spreading of the heat

to the inlet and outlet header area is expected, the area-averaged heat flux transferred is calculated based on the copper block area, A_H, as

$$\ddot{q} = \frac{Q}{A_H} \tag{3}$$

The cold plate base temperature or the junction temperature, T_J, was estimated using one-dimensional steady state heat conduction in the copper base plate:

$$T_J = T_B + \frac{\ddot{q}}{k_{CU}} \frac{t_B}{2} \tag{4}$$

where T_B is the measured temperature of the center of the finned area using the embedded thermocouple. The thermal conductivity of base plate, k_{CU}, was taken as 380 W/(m·°C).

The performance of the cold plate was evaluated in the terms of thermal resistance based on the inlet temperature difference method described in [14] as

$$R = \frac{T_J - T_{IN}}{Q} \tag{5}$$

The voltage was measured with an accuracy of ±0.05% and the current with an accuracy of ±0.1%.The uncertainties in power input to the heaters and thermal resistance, calculated by following the procedure of Kline and McClintock [15], was ±0.11% and between ±0.5 to ±4%, respectively.

RESULTS

The heat transfer data is represented in the terms of thermal resistance rather than heat transfer coefficient as the results pertain to a specific cold plate.

Single-phase water cooling

The thermal resistance decreases with the increase in water mass flow rate, $\dot{m}$, (Fig. 4). The dependence of thermal resistance can be represented $\dot{m}^{-0.4}$. The result is in close agreement with the correlation by Muzychka and Yovanovich [16] for laminar flow (Reynolds number less than 2300). Thermal resistance for turbulent flow (Reynolds number greater than 4000) is calculated using correlation by Gnielinski [17]. The thermal resistance for the transition regime is calculated by linear interpolation between the Muzychka and Yovanovich correlation at a Reynolds number of 2300 and the Gnielinski correlation at a Reynolds number of 4000.

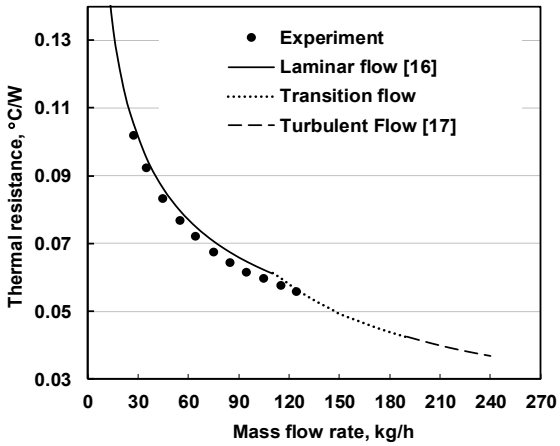

Fig. 4 Thermal resistance for water cooling

For the various test conditions, the relation of the pressure drop and thermal resistance of the cold plate is shown in Fig. 5. It can clearly be seen that the cold plate is not suited for achieving thermal resistance lower than 0.07 °C/W using water as the heat transfer fluid due to steep increase in pressure drop and associated pumping power.

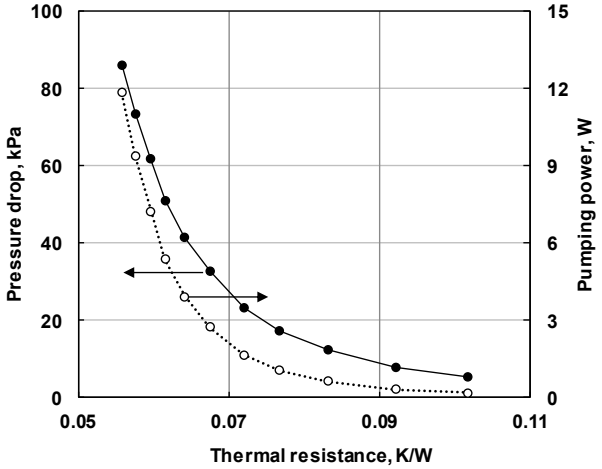

Fig. 5 Pressure drop versus thermal resistance for water cooling

Two-phase cooling

Figure 6(a) illustrates the effect of mass flux on the boiling curve plotted for R1233zd(E) based on the junction temperature and the saturation temperature at the inlet of the cold plate. The relation of heat flux with wall superheat can be represented by $\ddot{q} \propto \left(T_J - T_{SAT,IN}\right)^{1.75}$. It can be easily derived from this relationship that the two-phase heat transfer coefficient increases with heat flux, unlike single-phase cooling where the heat transfer coefficient is independent of the heat flux. The increase of heat transfer coefficient with heat flux can be either due to the increase in nucleation activity in the coalescing bubble flow regime or transition to wavy annular flow regime. It is difficult to arrive at any conclusion on the enhancement mechanism without performing flow visualization studies. This relationship between heat transfer coefficient and heat flux is beneficial for thermal management of electronic devices because the device temperature will not vary much with the workload of the device. A very weak dependence on mass flow rate on the boiling curve was seen, except at the lowest mass flow rates where the critical heat flux condition may have reached. However, Fig. 6(b) indicates that the thermal resistance decreases with increasing vapor quality and mass flow rate. Figure 6(c) shows that the pressure drop increases linearly with exit vapor quality and as square of the mass flow rate. The selection of flow rate will depend on the number of cold plates that are to be connected in series and the allowable saturation temperature drop. Increasing the mass flow rate increases the heat removal capacity of the flow stream but also increases the saturation pressure drop substantially, which reduces the available temperature difference in the condenser of the coolant distribution unit. For example, if the exit quality is under 80% at the end of the last cold plate in the cooling loop, a small amount of pumped R1233zd(E) (~10 kg/h) can easily remove heat from two inline heat loads of 200 W each with the total saturation temperature drop of less than 1 °C. The

shadowing effect will be eliminated as the fluid temperature at the inlet of the second cold plate will be same or lower than the saturation temperature of the fluid entering the first cold plate.

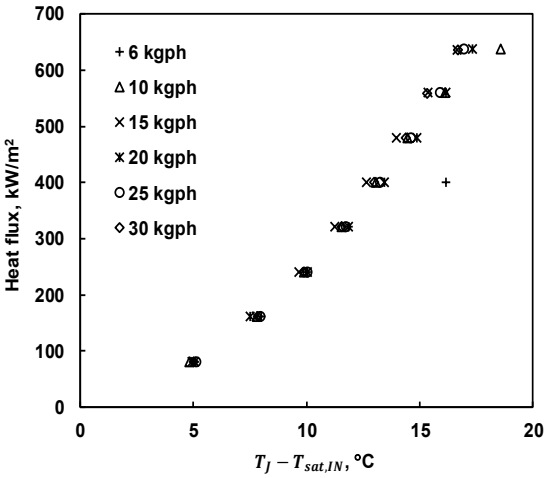

(a)

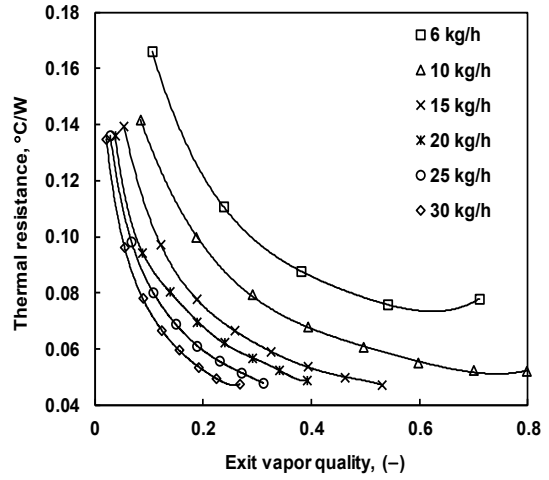

(b)

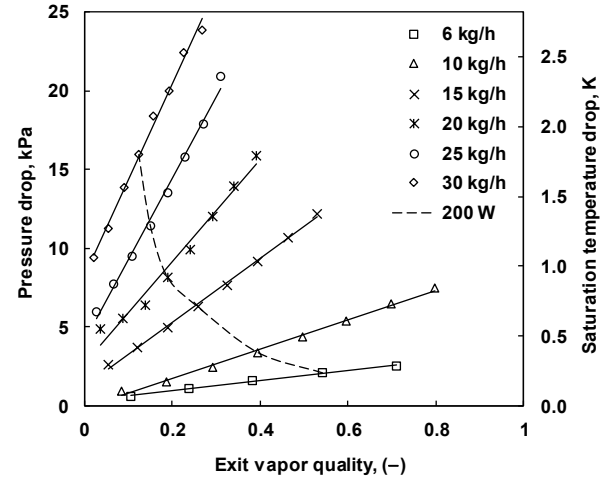

(c)

Fig. 6 (a) Boiling curve, (b) thermal resistance, and (c) pressure drop and corresponding saturation temperature drop for R1233zd(E)

Like R1233zd(E), boiling curve for both R1234ze(E) and R134a show a weak dependence on mass flow rate. The pressure drops for both R1234ze(E) and R134a are lower as compared to R1233zd(E) due to their lower liquid to vapor density ratio as compared to R1233zd(E). Thermal resistance of R1234ze(E) is 10-15% more than R134a.

Two-phase versus single-phase cooling

Figure 7(a) compares the junction temperature for power input in the range of 50 to 400 W at a flow rate of 30 kg/h. Additionally, the junction temperature for water flow rate of 80 kg/h and 170 kg/h were compared. R134a has the lowest junction temperature over the tested range of heat fluxes, closely followed by R1234ze(E). Junction temperature of water is highest at 30 kg/h, except at lowest heat input in this study. The thermal resistance of two-phase cooling relative to single-phase cooling with water also reduced with increasing power level (Fig. 7(b)).

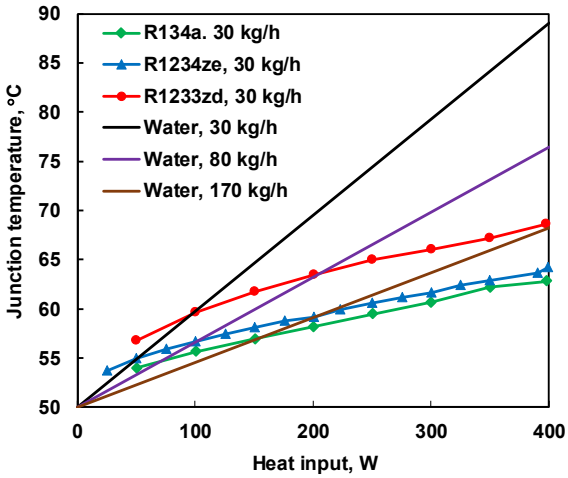

(a)

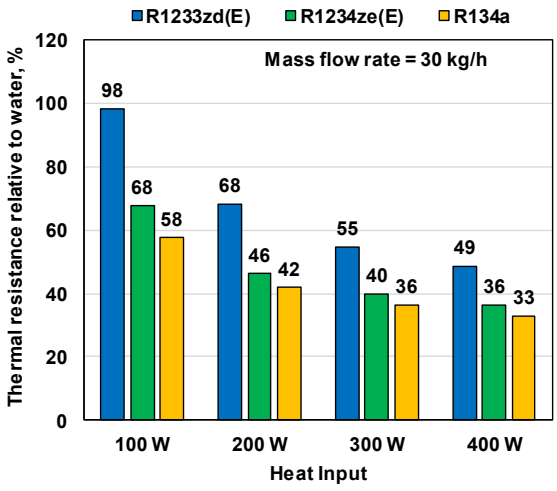

(b)

Fig. 7 (a) Junction temperature as a function of heat input, and (b) thermal resistance relative to water cooling

At heat input of 200 W, the junction temperature of water is only comparable with R1233zd(E) when its mass flow rate increased to 80 kg/h. At this flow rate, pressure drop and pumping power for water increased by 2.3 and 7.5 times, respectively, of R1233zd(E). Water is unable to match the

junction temperature of R1234ze(E) at the highest flow rate of this study. Using the turbulent flow heat transfer correlation of Gnielinski [17], it is predicted that the junction temperature of water at 200 W heat input will match that of R1234ze(E) only when its flow rate increases to 170 kg/h, and the resulting pressure drop would be almost 20 times of R1234ze(E).

Mashiko et al. [18] presented single-phase water cooling performance data for a parallel microchannel cold plate. Their cold plate required nearly 10 times higher effective microchannel surface area and 5 times larger finned area as compared to the cold plate evaluated in this study to achieve the thermal resistance of R1234ze(E) at 200 W heat input. Similarly, comparing the performance data of a water cooled cold plate in [19], it was determined that their cold plate required almost 20 times higher effective microchannel surface area to match R1233zd(E) performance obtained in the current study at 350 W heat input.

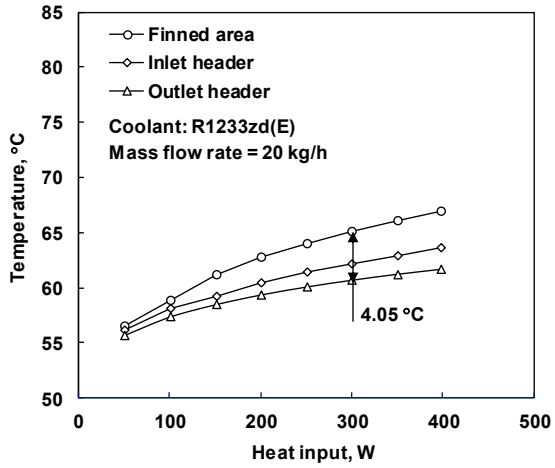

(a)

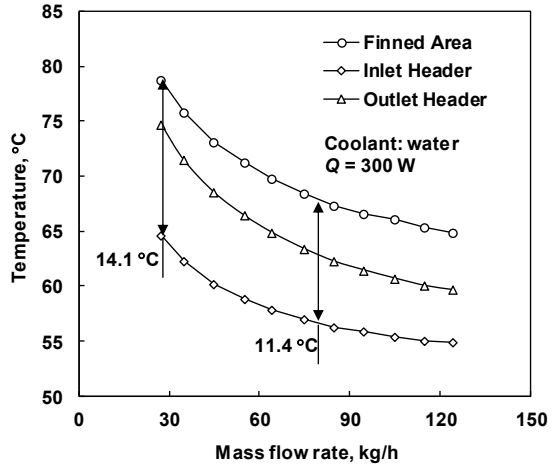

(b)

Fig. 8 Measured base plate temperature for (a) R1233zd(E) flow rate of 20 kg/h and (b) water cooling at 300 W heat input

It can be seen in Fig. 8(a) that even for R1233zd(E) at a flow rate of 20 kg/h, non-uniformity in base temperature at 300 W is much lower than that for water cooling with mass flow rate of 80 kg/h (Fig. 8(b)). While results are not shown here, temperature non-uniformity for R1234ze(E) and R134a is almost half of R1233zd(E). Figure 9 shows that the junction temperature change between idling (50 W) and maximum power (200 W) for two-phase cooling was also much lower than single-phase water cooling.

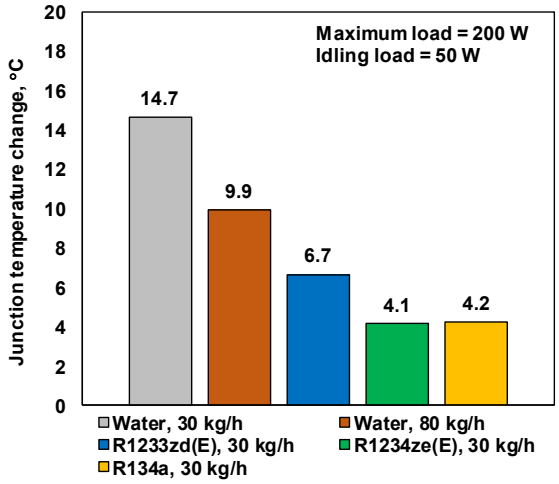

Fig. 9 Junction temperature change between maximum and idling heat load

CONCLUSIONS

In this work, it has been demonstrated that new ultra-low GWP dielectric fluids R1233zd(E) and R1234ze(E) can be used to cool current and future generation of CPU for HPC application with thermal dissipation power as high as 400 W per CPU. The use of two-phase cooling reduces junction temperature, temperature non-uniformity, junction temperature change between idling and maximum load, and pumping power as compared to single-phase cooling with water. While the thermal resistance decreases with increasing water flow rate in single-phase cooling, flow rates that are required to match the performance of two-phase cooling result in a steep increase in pressure drop and pumping power. On the other hand, two-phase cooling thermal resistance shows a weak dependence on mass flow rate but reduces with increasing heat input. The pressure drop shows a linear increase with vapor quality, i.e., increasing thermal load, but increases as a square of the mass flow rate. This property of two-phase cooling should minimize the effect of coolant maldistribution in the rack.

This study shows the attractiveness of two-phase cooling using R1233zd(E) and R1234ze(E) as long-term heat transfer fluids solutions that can meet the ever-increasing need for power density in HPC applications.

REFERENCES

[1] D. Kulkarni, X. Tang, S. Ahuja, R. Dischler, and R. Mahajan, "Experimental study of two-phase cooling to enable large-scale system computing performance," in 17th IEEE Intersociety Conference on Thermal and Thermomechanical Phenomena in Electronic Systems (ITherm), San Diego, CA, pp. 596-601, 2018.

[2] ASHRAE, "Water-cooled servers – common designs, components, and processes", Atlanta: ASHRAE Technical Committee (TC) 9.9, Mission Critical Facilities, Data Centers, Technology Spaces and Electronic Equipment., 2019.

[3] E. W. Lemmon, M. L. Huber, and M. O. McLinden, *Reference Fluid Thermodynamic and Transport Properties – REFPROP*, Ver. 9.1. NIST, Boulder, Colorado, 2013.
[4] C. L. Ong and J. R. Thome, "Macro-to-microchannel transition in two-phase flow: part 1 – two-phase flow patterns and film thickness measurements," Experimental Thermal Fluid Science, vol. 35, no. 1, pp. 37-47, 2011.
[5] R. Revellin and J. R. Thome, "Experimental investigation of R134a and R245fa two-phase flow in microchannels for different flow conditions," Int. J. Heat Fluid Flow, vol. 28, pp. 63-71, 2007.
[6] E. Costa-Patry, J. Olivier, and J. R. Thome, "Heat transfer characteristics in a copper micro-evaporator and flow pattern-based prediction method for flow boiling in microchannels," Frontiers Heat Mass Transfer, vol. 3, pp. 1-14, 2012.
[7] S. S. Bertsch, E. A. Groll, and S. V. Garimella, "A composite heat transfer correlation for saturated flow boiling in small channels," Int. J. Heat Mass Transfer, vol. 52, no. 7–8, 2110-2118, 2009.
[8] H. Huang, N. Borhani, and J. R. Thome, "Experimental investigation on flow boiling pressure drop and heat transfer of R1233zd(E) in a multi-microchannel evaporator," Int. J. Heat Mass Transfer, vol. 98, pp. 596-610, 2016.
[9] E. M. Fayyadh, M. M. Mahmoud, K. Sefiane, and T. G. Karayiannis, "Flow boiling heat transfer of R134a in multi microchannels," Int. J. Heat Mass Transfer, vol. 110, pp. 422-436, 2017.
[10] Y. Madhour, J. Olivier, E. Costa-Patry, S. Paredes, B. Michel, and J. R. Thome, "Flow boiling of R134a in a multi-microchannel heat sink with hotspot heaters for energy-efficient microelectronic CPU cooling applications," IEEE Transactions on Components, Packaging and Manufacturing Technology, vol. 1, no. 6, pp. 873-883, June 2011.
[11] J. A. Olivier and J. R. Thome, "Two-phase cooling of electronics with multi-microchannel evaporators," in AVT-178 specialists' meeting on system level thermal management for enhanced platform efficiency, Bucharest, Romania, 2010.
[12] D. Sharma, D. P. Ghosh, S. K. Saha, and R. Raj, "Thermohydraulic characterization of flow boiling in a nanostructured microchannel heat sink with vapor venting manifold," Int. J. Heat Mass Transfer, vol. 130, pp. 1249-1259, 2019.
[13] ASHRAE, Liquid cooling guidelines for datacom equipment centers, 2nd ed. Atlanta: ASHRAE, 2014.
[14] R. L. Webb, "Heat exchanger design methodology for electronic heat sinks," ASME. J. Heat Transfer, vol. 129, no. 7, pp. 899-901, 2007.
[15] S. J. Kline and F. A. McClintock, "Describing uncertainties in single sample experiments," Mechanical Engineering, vol. 75, pp. 3-8, 1953.
[16] Y. S. Muzychka and M. M. Yovanovich, "Laminar forced convection heat transfer in the combined entry region of non-circular ducts," ASME J. Heat Transfer, vol. 126, pp. 54-61, no. 1, 2004.
[17] VDI Heat Atlas, 2nd Edition, Springer-Verlag, Berlin Heidelberg, 2010.
[18] K. Mashiko, M. Mochizuki, K. Goto, M. Takahashi, M. Matsuda, Y. Horiuchi, and T. Nguyen, "Applications of cold plate units with micro-channel for cooling electronics," Proc. ASME 2013 InterPACK, Burlingame, CA, V002T08A001, July 16-18, 2013.
[19] J. Gullbrand, M. J. Luckeroth, M. E. Sprenger, and C. Winkel, "Liquid cooling of compute system," ASME. J. Electronic Packaging, vol. 141, no. 1, 010802, 2019.

DISCLAIMER